Applied Ocean Research 168 (2026) 104980

Contents lists available at ScienceDirect

Applied Ocean Research

journal homepage: www.elsevier.com/locate/apor

Definitions and characteristics of loading patterns on single and shared marine anchors for floating offshore wind turbines

D.J. White *, B. Cerfontaine, A. Rashidi Mehrabadi, S. Gourvenec

University of Southampton, United Kingdom

ARTICLE INFO

Keywords:
Offshore engineering
Anchor
Loading
Offshore renewable energy

ABSTRACT

The growth of floating offshore wind has prompted new attention on the behaviour of anchors, including the concept of anchor sharing among multiple mooring lines. A critical design interface is between the mooring line loads and the geotechnical design. Typically ten to a hundred design loading conditions must be rationalised into the critical contributions that govern the geotechnical response of the anchor.

This paper provides a framework to bridge between the mooring system analysis and the geotechnical design. Firstly, a methodology to translate a general time history of anchor loading into a characteristic 'fingerprint' is set out. This fingerprint has three components – (i) a 'heatmap' defining the normalised distribution of the cyclic loading across the three spherical dimensions of the resultant load, (ii) a vector of the relative cyclic frequency in these directions, and (iii) two scalar quantities required to unpack these normalised parameters to recover the original time series characteristics.

Secondly, measures of similarity are defined, that allow two fingerprints to be quantitatively compared. This provides a new measure to compare the idealised patterns of loading used in model testing, field testing or laboratory element tests with the more complex patterns that are found in real data of anchor loading or from numerical simulations of floating systems. The framework is illustrated by demonstrating the varying similarity evident between example mooring line loads and the common loading patterns applied in geotechnical testing.

In summary, this new framework allows anchor loading histories to be distilled into simple fingerprints and similarity measures, providing to tool to accelerate identification of critical design cases and allow more efficient idealisation for geotechnical modelling and design.

1. Introduction

1.1. Background and motivation

1.1.1. Anchor design for floating offshore wind

The growth of floating offshore wind to meet decarbonisation targets requires many thousands of marine anchors to be installed in the coming decades (Greaves et al., 2024; IRENA 2024). Supply chain constraints and the need to minimise material use and accelerate deployment mean that optimisation beyond current practice is required (Cerfontaine et al. 2023; Gourvenec 2024).

The general configuration of the anchor loading scenario for floating offshore wind installations is illustrated in Fig. 1a. A key optimisation is the use of shared anchors, in which multiple mooring lines are attached to the same anchor (Goldschmidt and Muskulus 2015; Fontana et al. 2016). Shared anchors are shown in Fig. 1a using the example of a hexagonal layout of anchors and floaters, such that each anchor is connected to three mooring lines at angles of 120° in plan. The use of shared anchors can reduce the number of anchors by up to 60 % (Fontana et al. 2016). Anchor sharing can also reduce the peak loads on the anchor relative to a single line case due to horizontal load components from different mooring line cancelling out. Numerical studies suggest this benefit could be a 30 % to 50 % reduction (Fontana et al., 2018; Pillai et al., 2022). However, the resulting load may be inclined more steeply upwards, which is more onerous, as the vertical load components are summed. Despite potential reductions in the peak load, shared anchors come at the expense of more complex multi-directional loading compared to single anchors, which could be detrimental to its cyclic performance (Cerfontaine et al. 2024).

Mooring lines may be taut – as shown in Fig. 1a – or in the form of a catenary, with a grounded section prior to the anchor. In addition, the mooring lines may incorporate load reduction devices, which aim to

* Corresponding author.
E-mail address: david.white@soton.ac.uk (D.J. White).

https://doi.org/10.1016/j.apor.2026.104980
Received 5 August 2025; Received in revised form 7 January 2026; Accepted 12 February 2026
Available online 23 February 2026

absorb peak loading events, leading to relief of extreme anchor loads (Festa et al. 2025).

The loading experienced by an anchor throughout the operating life is influenced by effects and events that range over many timescales (Fig. 2). These span from climate change-induced variations in the wind and wave conditions over the operating life of the facility (10^9 s) (e.g. Brown et al. 2019; Mosquera-Mosquera et al. 2020) through to short snatch loading events of around 10^0 s duration within a single cycle of wave loading (e.g. Hann et al. 2015; Lind et al. 2016). For a shared anchor, these loading events can lead to long term loading histories that are highly multi-directional, as well as cyclic (Fig. 1) (Pillai et al. 2022; Coughlan et al. 2025; Fontana et al. 2018). In design practice, these events are simplified into a set of Design Loading Cases (DLCs) based on international standards (IEC 2019; Lovera et al. 2025), which typically leads to between ten and a hundred load condition combinations that must be analysed.

The capacity of common anchor types under monotonic combined vertical and horizontal loading is well-established for drained or undrained soil properties (Randolph and Gourvenec, 2011; Aubeny, 2017). The added complexity of cyclic loading, leading to degradation and rate effects on soil strength, is captured at the soil element level by cycle-counting S-N fatigue-type methods (e.g. Andersen 2015), which can also be applied to an anchor under unidirectional line loading (Kwa et al., 2023). However, future floating wind installations require anchor capacity to be assessed allowing for two additional challenges: (i) multi-directionality of loading and (ii) whole life geotechnical effects. Current design guidance recognises these challenges, acknowledging, for example, that the "more complex cyclic loading pattern for shared anchors shall be considered when assessing cyclic soil strength degradation and the anchor holding capacity" (DNV, 2021).

1.1.2. Impact of loading multi-directionality and whole life soil response

Multi-directionality adds complexity to the resulting geotechnical response. For example, experiments show that two-directional planar loading can lead to faster accumulation of displacement than one-way cycles to the same maximum load (e.g. Leblanc et al., 2010), and generalisation to three-dimensional loading adds further complexity to the response (Rashidi-Mehrabadi et al., 2025). Experiments show that load multi-directionality can lead to greater accumulation of deformation compared to uni-directional loading with the same amplitude (e.g. Rudolph and Grabe 2013; Richards et al. 2020; Cerfontaine et al. 2024). Loading multi-directionality creates rotation of the principal stress directions in the ground, making this additional deformation consistent with element tests with principal stress rotation, which also reveal enhanced rates of strain accumulation, for both sand and clay (Miura et al. 1986; Mandolini et al. 2021; Cheng et al. 2023; Xiao et al. 2014). Meanwhile, multiple mooring lines attached to the same anchor cause the destabilising upwards vertical loads to be reinforced, even though combined horizontal loads may partly cancel (Fontana et al. 2018; Shimada et al., 2018).

Whole-life changes in soil strength can result from the operational cyclic loading followed by consolidation (Gourvenec 2020, 2022). These effects raise the stiffness and capacity of soft clays (Zhang et al. 2011; Zhou et al. 2020), and similar densification-related effects are observed in sand (Huang et al. 2020). Whole life effects can therefore provide a positive compensation for the detrimental influence of load multi-directionality.

To systematically address these two effects – multi-directionality and whole life strength changes – it is first necessary to quantify the anchor loading in a format suited to geotechnical analysis of capacity and soil strength over the operating life. Floating system analyses – which simulate the response of the floating unit and turbine under the actions

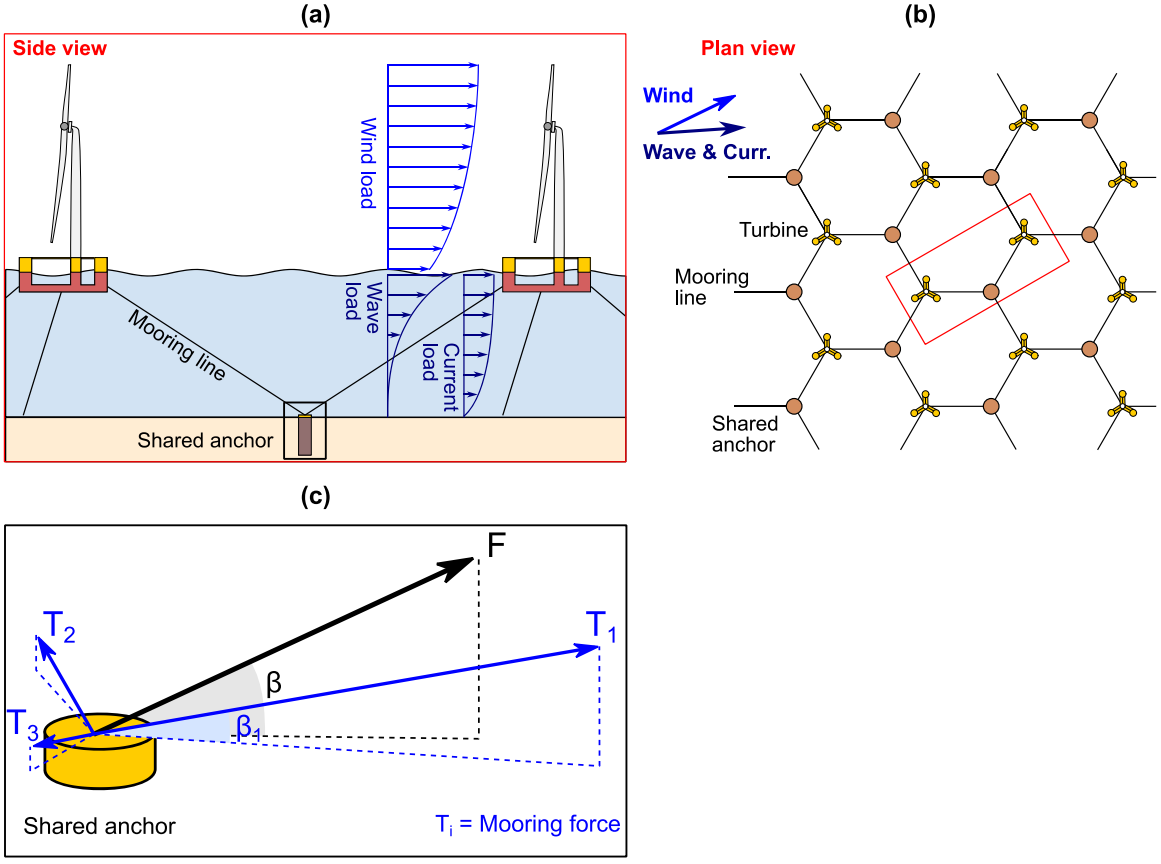

Fig. 1. Floating wind turbine system schematic: (a) Side view of two floating turbines and a shared anchor. (b) plan view of a wind farm connected to shared anchors. (c) Description of the resultant load applied to the shared anchor in cylindrical coordinates.

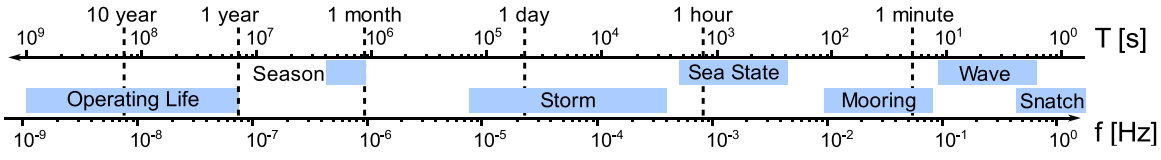

Fig. 2. Time periods relevant to whole life anchor loading.

of wind and waves – are used to ensure that the system meets the required design criteria set out by relevant standards (e.g. DNV 2021) or by the turbine manufacturer. These simulations also produce time histories of mooring line load at the anchor points, which are then used for geotechnical anchor design (DNV 2017a, 2017b, 2017c; ISO 2025). Geotechnical simulations – in physical experiments or numerical models – are necessarily idealised compared to the real multi-directional time history of loading. However, these idealisations must retain the key characteristics of the loading history that govern the geotechnical response.

1.2. Objectives

The objective of this study is to meet the requirement set out above, of quantifying an anchor loading history in a compact format, capturing key aspects relevant to geotechnical analysis and in a form that is convenient for comparison with experiments or other time histories. This is achieved by defining (i) the characteristic 'fingerprint' of a real or idealised anchor load history and (ii) measures of similarity to compare different histories, such as real and idealised examples. This methodological contribution provides a systematic approach to bridge from a floating system analysis (which generates a multi-directional anchor load time series for each design condition) to the idealised input for geotechnical analysis (either to perform design calculations, or to guide idealised physical or numerical simulations).

In Section 3 the anchor and mooring line system is defined, as well as the range of relevant timescales. In Section 4 typical time series data of anchor loading from a floating offshore wind system are introduced, for the interpretation set out in Section 5. This interpretation provides a general basis to convert an anchor loading history into a format suited to geotechnical analysis, capturing the aspects most critical to geotechnical behaviour. In Section 6 this same framework is used to illustrate the characteristics of typical idealised loading patterns that are used in geotechnical testing, to demonstrate how their consistency with realistic loading can be quantified. Measures to quantify the similarity between real and idealised load histories are described in Section 7.

1.3. Novelty and contribution relative to current practice

The key novelty contributed by the 'fingerprint' methodology of this study is the capability of quantifying in a compact way the multi-directionality of a loading time history, and to capture this in a format that allows rapid comparison of multiple loading cases. Conventional rainflow analysis of a single load time series neglects multi-directionality. Meanwhile, conventional damage accumulation methods – such as S-N curves – can be used to compare the impact of different load cases, but they require geotechnical parameters, whereas the fingerprint concept is based only on the loading history.

This ability to consolidate a series of loading histories into a set of simple fingerprints that can be efficiently compared addresses the challenge of analysis overload that is associated with floating system design. Current design procedures lead to a large number of design load cases (DLCs), and it is common practice to generate multiple time series load histories using different seeds for each DLC. It is impractical to conduct a geotechnical design analysis for all load histories from all DLCs. Instead, by clustering load cases and time histories using fingerprints, and analysing a representative selection, the relative severity and design criticality can be more efficiently determined.

This loading fingerprint concept is complementary to the geotechnical practice of damage accumulation (or cyclic strength degradation) by S-N curves (which results, primarily, in a loading history being converted to an equivalent number, N_{eq}, of the largest cycle (Andersen 2015)). These accumulation procedures require defined geotechnical parameters (and an estimate of the foundation or anchor capacity), which are used to normalise and shape the S-N curves and therefore set the damage or N_{eq} from a given load history. The fingerprint approach in this paper is based only on the loading history, not any specific geotechnical properties, so can be performed prior to the selection or definition of any geotechnical design parameters of anchor dimensions. As discussed at the end of the paper, experience gained from S-N analyses of the fingerprint outputs may help identify which aspects of the fingerprint are most closely linked to the geotechnical performance. This could lead to improved definition of the fingerprints.

1.4. Applicability

The fingerprint methodology is applicable to all anchors – single or shared – since the loading is defined using a general formulation that allows full multi-directionality (i.e. the direction of the resultant load can vary throughout the half space above the horizontal seabed). Planar loading is a special case in which one of the loading angles (defined later) remains constant, and uni-directional loading is a further special case in which both loading angles remain constant. Loading on a single anchor is usually slightly multi-directional, because of vertical variations in the loading direction if the mooring line is lifted from the seabed and vertical or lateral variations due to movement of the floating unit. However, loading on a single anchor can sometimes be idealised as uni-directional or planar, if one or both of these effects are negligible. Loading on a shared anchor is usually strongly multi-directional as the most heavily loaded mooring line changes during a seastate or between subsequent seastates (which may have different wind or wave directions).

2. Anchor, mooring system and loading period definitions

The geometry and notation of the loads on an anchor from the attached mooring lines is defined in Fig. 1c. The resultant of the applied tensions can be defined as a single force vector, using the geometry and notation in Fig. 3. The present analysis is concerned only with a connection point (padeye) located on the top of the anchor, at which all mooring lines are attached. The analysis could be extended for alternative padeye positions, noting that moment actions are created if the

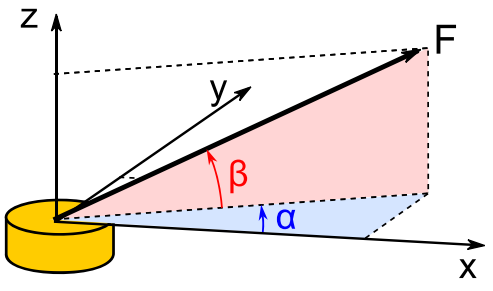

Fig. 3. Geometry and notation to define resultant force on anchor.

load vectors from the mooring line do not pass through a single load reference point. While a top pad-eye is not commonly used due to the lower capacity compared to an embedded pad-eye (Randolph and Gourvenec 2011), it can be favoured from an integrity management perspective (Foglia et al. 2025).

The cartesian coordinate system, xyz, is centred at the anchor connection point (Fig. 3). It is convenient to align the x-axis in the horizontal direction of the initial configuration of the mooring line, for a non-shared anchor (but this choice does not affect the outcome). For a shared anchor, this could be the most heavily-loaded line.

The applied mooring line loads are converted to spherical co-ordinates, with the horizontal direction anti-clockwise from the x-axis defined as α and the vertical inclination upwards from horizontal being defined as β. The resultant force is F.

The time periods relevant to loading actions on a floating offshore wind turbine span from 10° to 10^{9} s, from snatch loads to the entire operating life (Fig. 2). Floating system analyses are conducted for each Design Load Case (DLC), which involves a single seastate – defined as a stationary set of metocean conditions, typically lasting for 3 h. Within that simulation, all of the shorter period actions ($<10^{4}$ s) are found, down to the brief snatch loads, if applicable. The longer period effects – such as seasonality, or the variation between storm directions – are considered in structural fatigue analyses that accumulate the effects of many different DLCs, seastates and storm events, which comprise a whole life of loading (e.g. Liao et al. 2022). The recognition that loading history can affect soil properties means similar analyses that accumulate the effects of many DLCs and sea states are also emerging for the fatigue of monopiles (e.g. Schafhirt et al. 2016; Ma et al. 2024) and changes in the stiffness and capacity of foundations and anchors (Gourvenec 2020; Lai et al. 2020; Kwa et al., 2023).

3. Example floating system analyses

Two time histories of anchor loading derived from a time domain simulation of a floating wind turbine in a typical design seastate (i.e. of duration ~104 s) are used as exemplars to illustrate the interpretation framework that simplifies the loading into the critical characteristics relevant to geotechnical analysis. Both time histories are from the study of Coughlan et al. (2025), based on the Volturn steel semi-submersible supporting a NREL 15 MW wind turbine, moored via a taut line system (Coughlan et al., 2025; Allen et al. 2020). This case study was selected due to being very recent and well-documented, with publicly-available mooring loads, and using a wind turbine and platform that match current commercial sizes. Two histories are used: (i) an anchor with a single mooring line attached and (ii) a shared anchor with three mooring lines attached, each from different floating units (Coughlan 2025).

The platform is located in 850 m water depth – to represent typical US West Coast conditions – with a taut mooring system of three lines comprised of steel wire and chain. The simulations, using the OpenFAST 3.3.0 software (Coughlan et al. 2025; Jonkman and Sprague, 2026), subjected the platform to a seastate represented by the JONSWAP spectrum. In this paper, we use the loading time history for design load case DLC6.1, when the turbine is parked. This has a significant wave height $H_s = 10.8\ m$ and peak period, $T_p = 15.1\ s$ concurrent with a mean wind speed of 36.5 m/s and a surface current equal to 1.49 m/s. A fixed pin located 1155 m radially from the platform centre represented the anchor point, resulting in a mooring line angle of $\beta = 36$ degrees.

The resulting time histories are shown in Fig. 4, in terms of the resultant cartesian forces applied at the anchor load reference point, (F_x, F_y, F_z). The x-axis is aligned with the direction of the mooring line for the single line case, and in the direction of the windward mooring line, which is the most heavily loaded, for the shared anchor case. Throughout the time history, $\frac{F_z}{F_x} \approx 0.75$ due to the mooring line inclination, and $F_y \approx 0$ due to the floter movement being negligible, so the mooring line remains perpendicular to the y-axis.

4. Interpretation of mooring loads for geotechnical analysis

4.1. Introduction

A general multi-directional mooring time history, as shown in Fig. 3, can be systematically characterized for geotechnical analysis purposes via the following quantities, which are explained in sequence:

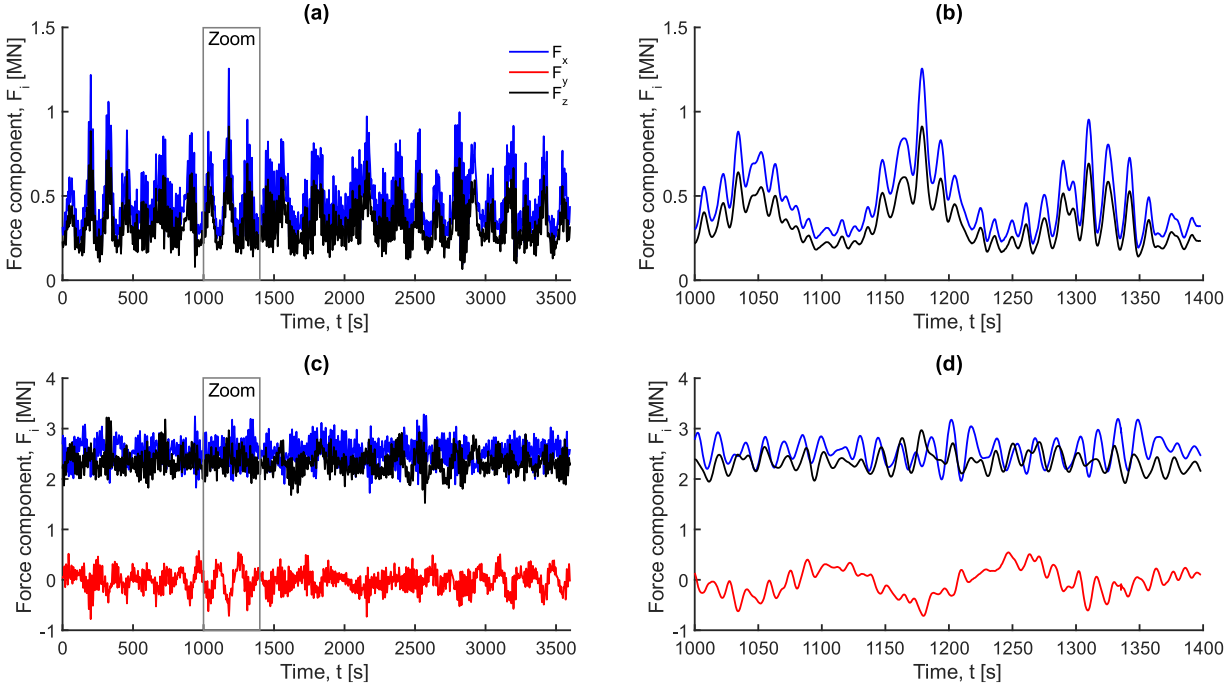

Fig. 4. Time histories of resultant mooring line loading in cartesian reference frame (a -b) Anchor with single mooring line, (c-d) Shared anchor.

(a) Mooring line loads are firstly synthesized into spherical loading parameters – which captures the overall load on the anchor, F, and uses the angle β to distinguish between load components that mobilise axial resistance and lateral resistance at the anchor, acknowledging that these geotechnical responses are different and often treated separately (Section 5.2).
(b) Temporal distributions are generated to quantify the weighted range of the loading parameters, F, α and β, indicating the loading domain space occupied by the loading history (Section 5.3).
(c) Rainflow cycle counting is used to identify, for each loading parameter, the distribution of the mean and cyclic amplitude of the cycles, and the relative number of cycles of each loading parameter (Section 5.4).
(d) The frequency spectrum of each loading parameter is also generated (Section 5.5).

All of these characteristics have a role in identifying, in a simple way, the 'fingerprint' of a loading time history relevant to geotechnical analysis. Together, the characteristics allow the similarity between idealized and actual loading histories to be quantified, as shown later.

4.2. Definition of spherical loading parameters

A spherical coordinate system, centred at the anchor load reference point, captures directly the changing direction and resultant load, $\underline{F}$, on the anchor, which are not evident in individual cartesian coordinates. The spherical load parameters are:

$$\underline{\boldsymbol{F}} = \begin{pmatrix} F \\ \alpha \\ \beta \end{pmatrix} = \begin{pmatrix} \left(F_x^2 + F_y^2 + F_z^2\right)^{1/2} \\ \text{atan}\left(\dfrac{F_y}{F_x}\right) \\ \text{atan}\left(\dfrac{F_z}{\left(F_x^2 + F_y^2\right)^{1/2}}\right) \end{pmatrix}$$

where F is the resultant force from the mooring line(s), α is the direction of F in the horizontal plane, measured anticlockwise from the reference direction, $\alpha = 0$ and β is the upward inclination of F from the horizontal plane (Fig. 1c).

The components of $\boldsymbol{F}$ can be normalized between zero and unity using the maximum resultant load in the time series, F_{max}, and the maximum possible ranges of each angle, which are $\alpha_{max} = \pi$ and $\beta_{max} = \pi/2$. However, it can be preferable to display the angles without normalization, which remain dimensionless and have clear physical meaning. The $\alpha = 0^\circ$ axis is parallel to F_x, which is aligned with the single mooring line, or the most heavily-loaded line for the shared anchor. For arbitrary time histories, or a situation where the most heavily-loaded line is unknown or varying between sea states, the $\alpha = 0^\circ$ axis can be defined as the average horizontal direction of the resultant force, such that the time-averaged angle $\overline{\alpha} = 0^\circ$.

The time series shown in Fig. 4 are illustrated using spherical parameters in Fig. 5.

Key characteristics of the single mooring line case that are evident in Fig. 5 are (i) a mean resultant anchor load, F, that is approximately 30 % of the peak value, (ii) a consistent inclination of loading, at $\beta \sim 36^\circ$ (iii) superposed cyclic components with periods that represent wave action (~10 s) and the natural period of the platform-mooring system (~150 s). For the shared anchor with three mooring lines, key features are (i) a higher vertical inclination of the resultant load (higher β)compared to the single line case due to reinforcement of the upwards components from multiple mooring lines (while the horizontal components partially cancel out), and (ii) high variations in the loading direction in the vertical (β) and horizontal planes (α), reflecting the alternating influence of tension in different mooring lines.

4.3. Time distributions of loading parameters: temporal heatmaps

To summarise the distribution through time of the loading parameters, each parameter is presented as a single distribution (Fig. 6a-c), and as bi-variate distributions ('heatmaps') (Fig. 6d-h) that show pairs of parameters. These illustrate the range of each parameter – with a log scale used to highlight extreme tails (low: Fig. 6b, high: Fig. 6c) – and how they correlate with each other.

Bi-variate distributions using the spherical parameters are shown in

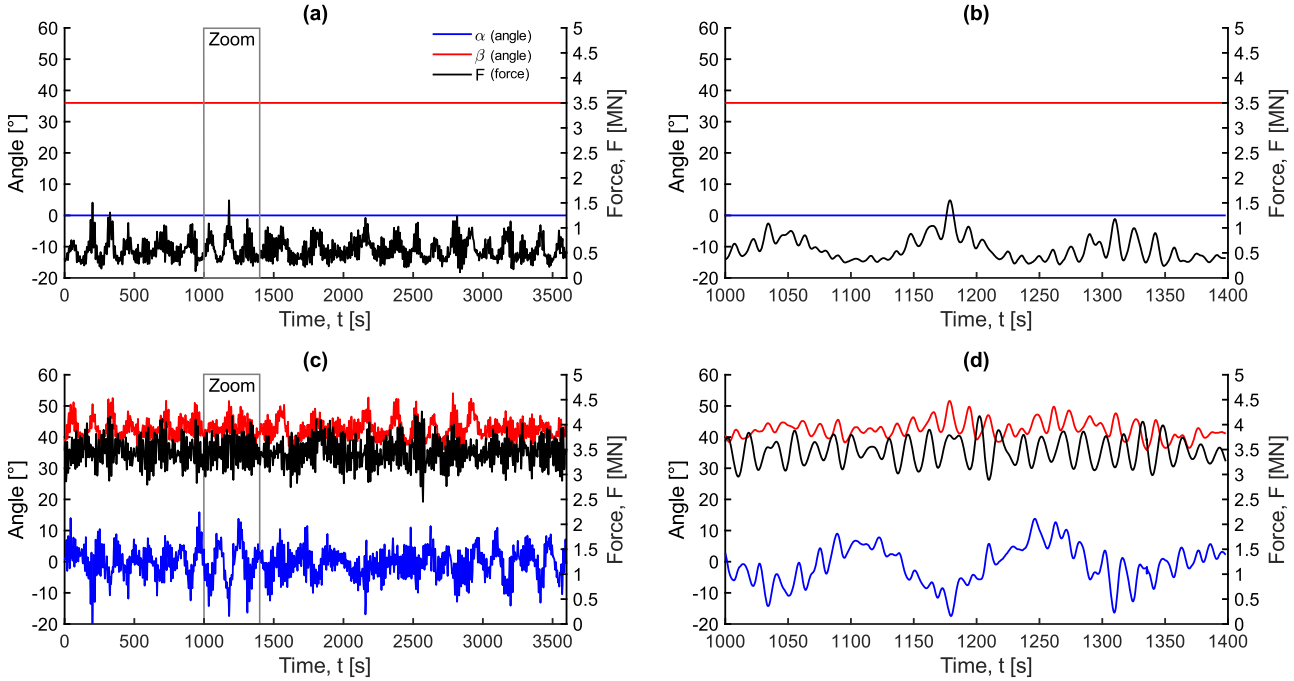

Fig. 5. Time histories of loading in spherical load parameters (a -b) Anchor with single mooring line, (c-d) Shared anchor.

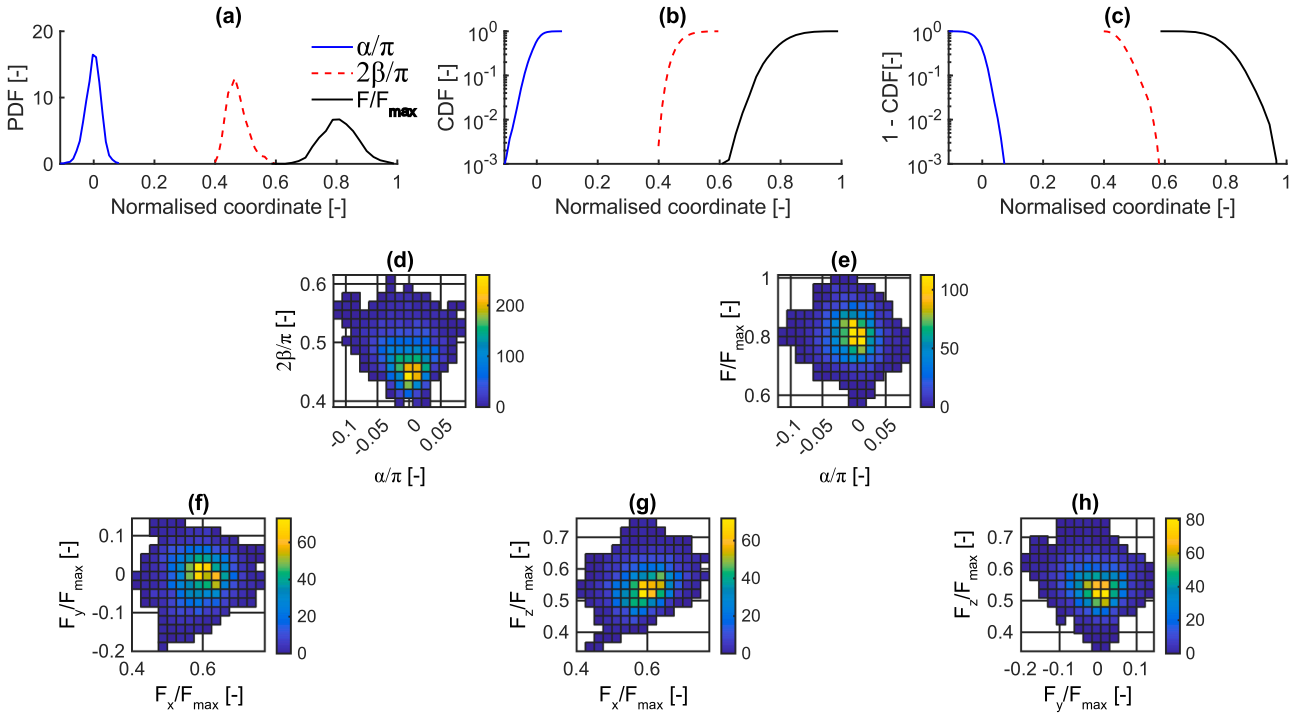

Fig. 6. Distributions of loading parameters for shared anchor case: (a-c): Univariate ranges of F, $\boldsymbol{\alpha}$ and $\boldsymbol{\beta}$; (a) Distributions, (b) Cumulative distributions (CDFs) showing low tail, (c) (1- CDFs) showing high tail, (d)-(f) Bivariate ranges; (d) angular range ($\boldsymbol{\alpha}$, $\boldsymbol{\beta}$) parallel to x-axis (primary mooring line), (e) 'plan' view in spherical coordinates, ($\boldsymbol{R}$,$\boldsymbol{\alpha}$), (f) cartesian ($\boldsymbol{x}$,$\boldsymbol{y}$) plan view, (g) cartesian ($\boldsymbol{x}$,$\boldsymbol{z}$) perpendicular to x-axis (primary mooring line) and (h) cartesian ($\boldsymbol{y}$,$\boldsymbol{z}$) parallel to x-axis (primary mooring line).

Fig. 6d-e. These illustrate that the maximum resultant force coincides with an orientation of $= 0, \frac{2\beta}{\pi} = 0.43 (\beta = 38.7^{\circ})$. A lower resultant force is applied at the adjacent range of α (Fig. 6e). The angle β varies only slightly below the orientation of peak force, but varies widely across higher values, up to $\frac{2\beta}{\pi} = 0.6$ $(\beta = 54^{\circ})$ (Fig. 6d). Other bi-variate distributions, based on the cartesian parameters, provide a useful representation of the loading history in planes that are parallel and perpendicular to the $\alpha = 0^{\circ}$ axis and in plan (Fig. 6f-h).

These type of loading heatmaps provide an efficient way to visualize the effect of metocean and mooring system parameters on the temporal distribution of anchor load. However, they do not indicate the number and nature (i.e. the mean and cyclic amplitude) of the loading cycles, which are critical to the geotechnical response, since they drive pore

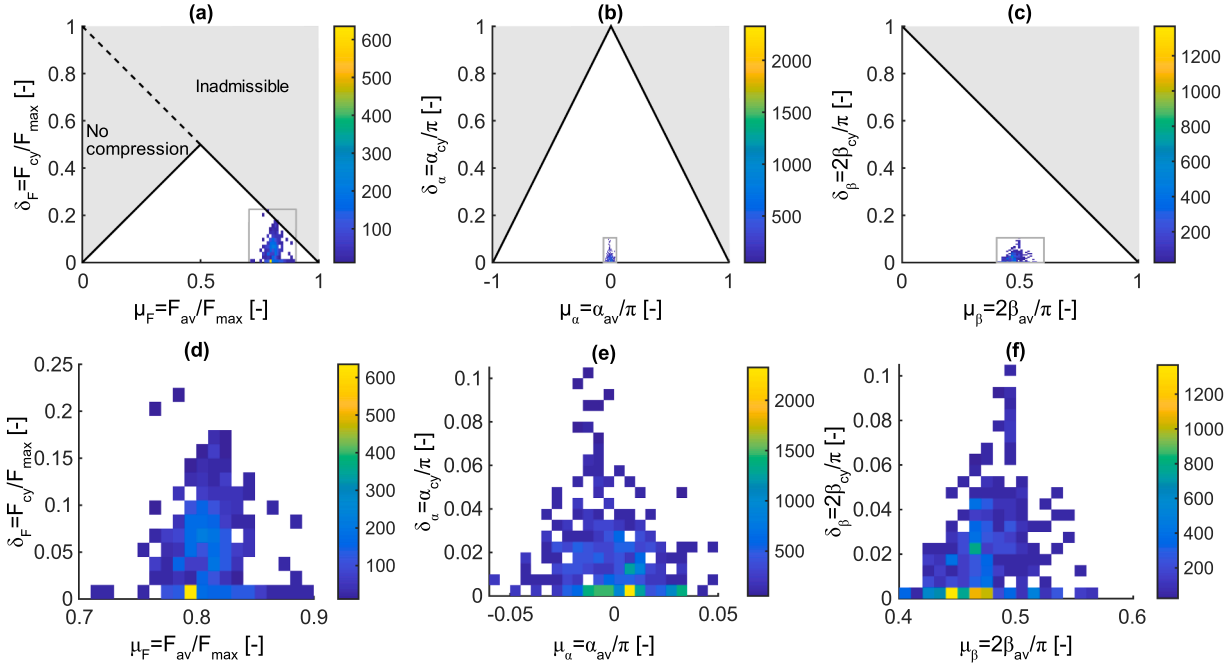

Fig. 7. Cyclic loading distributions, $\boldsymbol{\psi}$, for shared anchor case (second plot shows inset zone indicated on first plot): (a,d) Resultant force, $\boldsymbol{\psi_F}$, (b,e) Horizontal angle, $\boldsymbol{\psi_\alpha}$, (c,f) Vertical angle, $\boldsymbol{\psi_\beta}$.

pressure generation or densification. Geotechnical analyses of soil softening or densification use accumulation routines based on these cyclic parameters (e.g. Andersen 2015), rather than on the temporal variation of load level.

4.4. Cycle counting of loading parameters: cyclic heatmaps

To capture this cyclic information, a rainflow counting procedure (ASTM 2017) is applied to each of the spherical parameters of $\boldsymbol{F}$, resulting in a population of cycles, each with a mean (F_{av}, α_{av} or β_{av}) and a half-amplitude $\left(F_{cy}, \alpha_{cy} \text{ or } \beta_{cy}\right)$ that can be normalized by the ranges, $(F_{max}, \pi, \pi/2)$ to give dimensionless values, e.g. $\mu_F = F_{av}/F_{max}$ and $\delta_F = F_{cy}/F_{max}$. These populations of cyclic means and amplitudes are collated into cyclic heatmaps defined as the normalized cyclic distribution functions (denoted $\psi_F(\mu_F, \delta_F)$, $\psi_\alpha(\mu_\alpha, \delta_\alpha)$ and $\psi_\beta(\mu_\beta, \delta_\beta)$) (Fig. 7). These distributions show how the cycle population is distributed across the range of mean and cyclic amplitudes, in a form that is independent of the overall length of the input time history.

It is usual in geotechnical analysis for the static or monotonic capacity (e.g. F_{ult}) to be used for normalization of these axes of Fig. 7, but these heatmaps relate only to the loading and are independent of any anchor characteristics. The ψ_F heatmap would become a stability diagram for a specific anchor of capacity F_{ult} if each axis was scaled down by the relevant combined partial factors, i.e. $\frac{F_{ult}}{F_{max}} = \gamma_r \gamma_a$ using partial factors on geotechnical resistance, γ_r and total load, γ_a.

To complete the cycle counting interpretation it is necessary to quantify the different mean frequencies of the cycles of each loading parameter. Each cyclic parameter heatmap (Fig. 7) is normalized to a volume of unity, but the underlying loading time series will not in general feature the same number of cycles of each parameter in $\underline{\boldsymbol{F}} = (F, \alpha, \beta)$. The relative cyclic frequency of the three components, $\omega = \left(\omega_F, \omega_\alpha, \omega_\beta\right)$ is simply the relative number of cycles of each component, scaled to unity for the most frequent component. This vector can be illustrated by a spider diagram (Fig. 8a) and similar plots can be produced for the cartesian axes (Fig. 8b). These diagrams indicate the relative number of cycles in each component of $\underline{\boldsymbol{F}}$ within the time history.

By sampling the cyclic distributions ($\psi_F, \psi_\alpha, \psi_\beta$) in ratios corresponding to their relative frequency, ω, loading histories can be generated with the same cyclic content as the original time series, for geotechnical cyclic accumulation analysis. To fully recover the cyclic content of the original time series, the required total number of cycles must be defined. This information is defined by the rate that cycles occur, adopting the most frequent component, f_p (defined as the total number of cycles from the rainflow analysis, divided by the period of the time series). The relative frequency vector, ω allows f_p to be scaled to the other components.

For the shared anchor time history the two scalar parameters that complete the analysis were $F_{max} = 4.26\ MN$ and $f_p = 0.11\ Hz$ (which corresponds to the parameter α).

The final form of presenting the cyclic content of the loading history is via bi-variate heatmaps that classify the cyclic nature of individual cycles across all three parameters in $\underline{\boldsymbol{F}}$. These maps cannot be generated from the data in Fig. 7, because the individual cycles of each parameter occur over different intervals of time. Instead, the bi-variate nature of the cycles must be determined from a rainflow analysis on one specific loading parameter, which is chosen as F. From this F-rainflow analysis, the mean and range of α and β in each cycle of F are extracted, and used to form bi-variate distributions that illustrate the variation in all three spherical loading parameters during the cycles of F (Fig. 9). These distributions of mean values (Fig. 9a-c) show that there is a dominant zone of μ_F, μ_α and μ_β that represents a large proportion of the cycles. In contrast, the half-amplitude ranges δ_F, δ_α and δ_β are more widely distributed, and include an isolated population of very small values.

Since these distributions are from the F-rainflow analysis, the α and β ranges in a cycle are not between maxima or minima, and the start and end points will not generally be the same force vector. To illustrate this, six individual cycles from the F-rainflow analysis are shown in Fig. 10. The cycles are shown in Cartesian plan and vertical plane projections (where $F_h = \left(F_x^2 + F_z^2\right)^{1/2}$) in Fig. 10a-b. This format reveals the complex nature of these cycles, which are three-dimensional open loops. The shapes can be linked to the different frequencies of the three spherical components, which are shown as time histories in Fig. 10c-e. As an F-rainflow analysis, each cycle extends between maxima or minima of F. However, the angles typically have slightly higher frequency on average (as captured in Fig. 8a) causing the force vector to rotate about the load origin during each cycle. Some F-cycles are accompanied by a net drift in α or β, and vice versa, due to the range of frequencies present.

4.5. Frequency spectra of loading parameters

The final interpretation of the time histories is a simple frequency analysis on each parameter of $\underline{\boldsymbol{F}}$. The Fourier power spectra of each parameter are shown in Fig. 11. For the single mooring line case, this shows clearly the two dominant frequency ranges at the wave period and the natural period of the mooring system. However, this information is less relevant to geotechnical testing and analysis compared to the cycle counting of Section 5.4. This is because the primary influence of loading rate is to determine whether undrained or drained conditions are required. These are typically bounded by rates defined to the order of magnitude due to uncertainty in the coefficient of consolidation that controls drainage rate (e.g. Finnie and Randolph 1994), rather than being contingent on the narrow range of frequencies evident in Fig. 11.

The geotechnical response in undrained conditions is weakly influenced by viscous rate effects, which typically increase the resistance by 10 % per log cycle of strain rate (e.g. Sheahan et al. 1996; Biscontin and Pestana 2001), and also by inertial forces resulting from mass accelerations (e.g. Kwa et al., 2021). However, these effects usually have only a

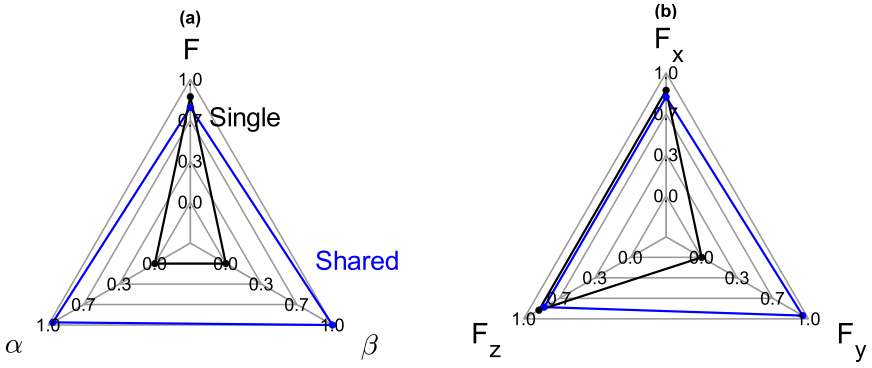

Fig. 8. Relative cyclic frequencies: (a) spherical parameters, (b) cartesian parameters.

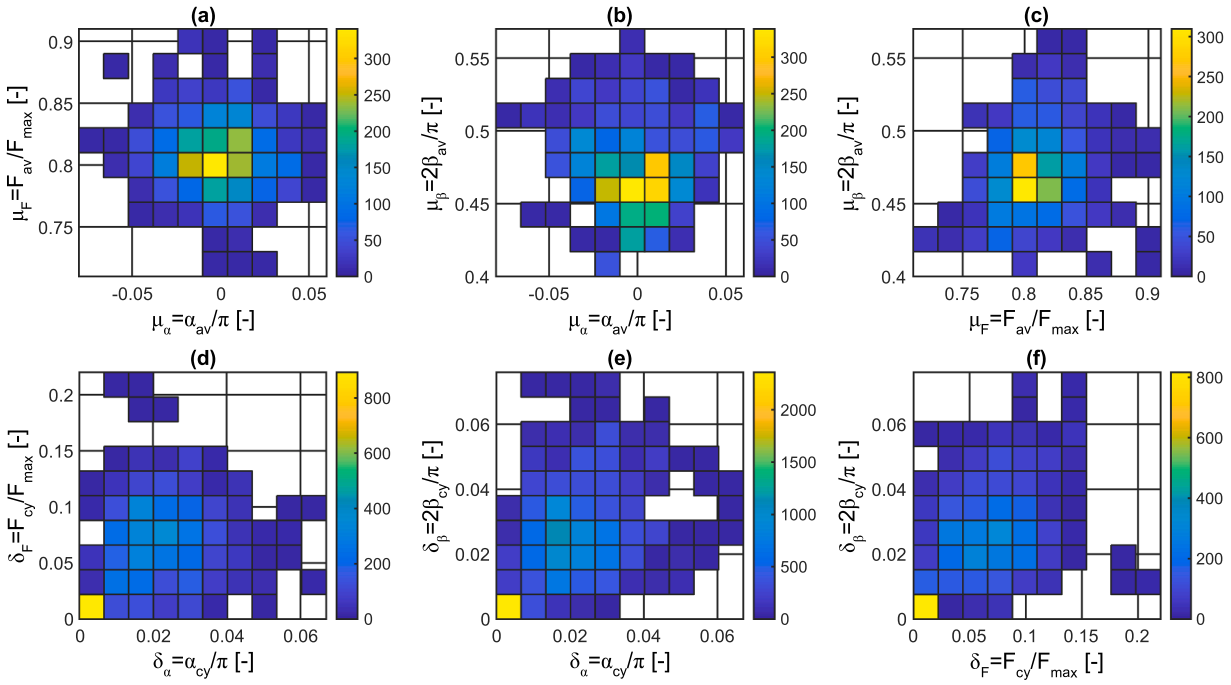

Fig. 9. Bi-variate distributions of cyclic parameters (based on ***F***-rainflow) (a)-(c) Pairs of average value, ($\boldsymbol{F_{av}}$,$\boldsymbol{\alpha_{av}}$, $\boldsymbol{\beta_{av}}$); (d)-(f) Pairs of cyclic amplitude, ($\boldsymbol{F_{cy}}$,$\boldsymbol{\alpha_{cy}}$,$\boldsymbol{\beta_{cy}}$).

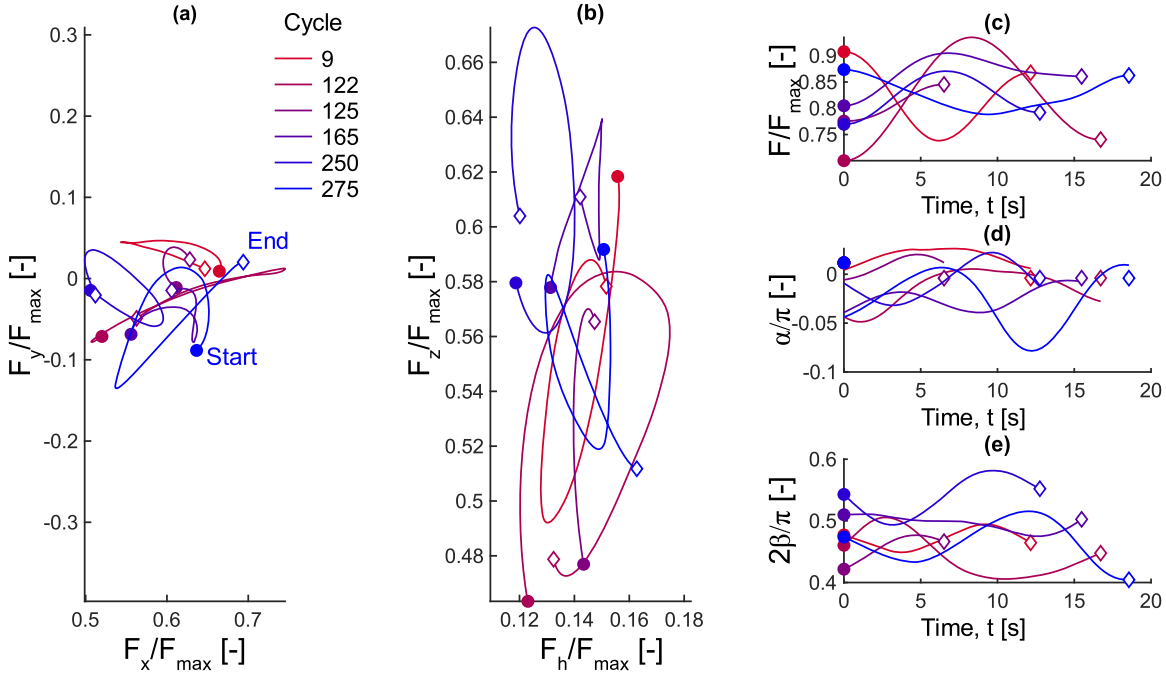

Fig. 10. Examples cycles for shared anchor case (from F-rainflow analysis): (a) Cartesian plan view, (b) Cartesian vertical plane projection, (c)-(e) Time variation of spherical parameters, (***F***, **α**, **β**).

secondary influence on the geotechnical response, so the frequency spectrum is not an essential characteristic of the loading history for geotechnical analysis.

4.6. Summary

To summarise, a general anchor loading time history of any duration – such as the examples shown in Fig. 4– can be summarised via the normalised heatmaps and distributions of Fig. 6 to Fig. 11. For geotechnical analysis purposes, Fig. 7 and Fig. 8 alone (plus the scalars F_{max} and f_p) provide a 'fingerprint' that contains all the information relevant to geotechnical analysis, namely the number and nature (mean value and amplitude) of all cycles during a given time period, defined in each of the spherical coordinates. The only information lost in this format is the correlation between cyclic parameters in each spherical dimension, which influences the 'shape' of individual cycles. This information is contained in the *F*-rainflow bi-variate heatmaps (Fig. 9).

By sampling from the cyclic distributions of Fig. 7 and Fig. 8 the random realisations of the loading parameter distributions can be generated (Fig. 6), and shown in either spherical or cartesian

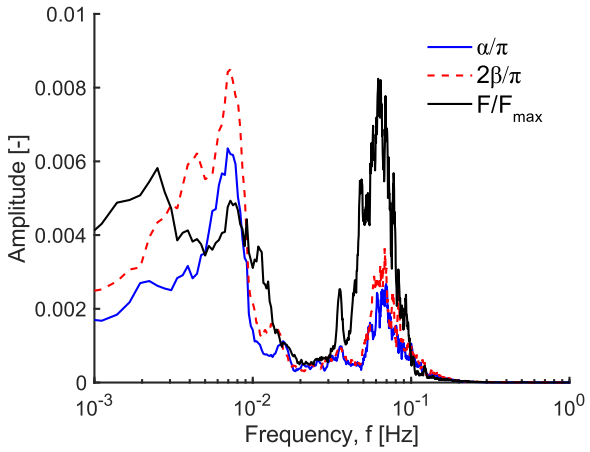

Fig. 11. Frequency distribution of spherical parameters.

coordinates (with the latter assisting in visualisation of the loading patterns).

Compared to the heatmaps from the cycle-counting, the actual frequency spectrum of the loading (Fig. 11) is usually of secondary importance in the geotechnical analysis. However, this can be relevant in circumstances where viscous rate effects or inertial effects influence the geotechnical response, or if drainage and consolidation occur during the cycles of loading.

5. Idealised loading paths used in geotechnical testing

The interpretation framework set out above can be applied to the idealised load paths used in geotechnical testing, as well as to loading histories from floating system simulations. The following analysis provides an overview of several such idealised load paths and shows how the framework captures their differing characteristics.

Some examples of single idealised cycles are shown in Fig. 12, simplified to only the $F-\alpha$ horizontal plane. Two closed loops are shown, defined as an ellipse (marked (1)) or straight line (4) in Cartesian plan coordinates (Fig. 12a). These are formed by a single cycle of α and a single (ellipse) or double (line) cycle of F. In contrast, if the frequencies of F and α differ, such that a single cycle of one is accompanied by a monotonic drift of the other, then open loop 'Z' (2) and 'tooth' (3) cycles are formed (Fig. 12). These examples illustrate how idealised cycles can be tailored via the relative frequencies of the spherical components to mimic the types of open loop cycles seen in the shared anchor time series (Fig. 10).

Five idealised load paths are summarised in Table 1 and illustrated in Fig. 13, all of which have been used in previous studies, although not necessarily to represent single-line or shared anchor responses. In some cases the paths were intended to represent the loading on a fixed structure or were defined to suit calibration of a predictive model. The interpretation framework has been applied to these idealised load paths to define the 'fingerprint' given by the cyclic distribution functions, ψ, in spherical parameters as well as the relative cyclic frequencies, ω (Fig. 14). For simplicity, all the idealised paths are multi-directional but only in the horizontal plane (i.e. $\beta = 0$ throughout).

6. Load history similarity analysis

The interpretation framework summarized by Fig. 7 and Fig. 8 is

Table 1
Idealised multi-directional load paths used in geotechnical testing.

Name	Notes and references
T-shaped (Fig. 12a)	A constant load offset with a perpendicular cyclic component (can be considered as a degenerate ellipse, with zero minor axis). Used in field tests (e.g. McAdam et al. 2024), physical modelling (e.g. Richards et al. 2020) and numerical simulations (e.g. Levy et al. 2009).
Offset spiral (Fig. 12b)	A non-offset spiral, used in experiments as a challenge for modelling rather than to represent realistic loading (Richards 2019). The offset spiral used here is shown later to be a promising representation of realistic loading.
Fan (Fig. 12c)	Represents conventional one-way cyclic loading, but with slowly-varying direction α. Used in model testing (e.g. Rudolph and Grabe 2013, Richards et al. 2020).
Shell (Fig. 12d)	Covers same loading domain as the fan, but with the path of the resultant load rotated by 90 degrees, and the relative frequencies of α and F reversed.
Random ellipses (Fig. 12e)	Ellipses with varying centre and major and minor axes, spanning a similar load region as the fan and shell examples

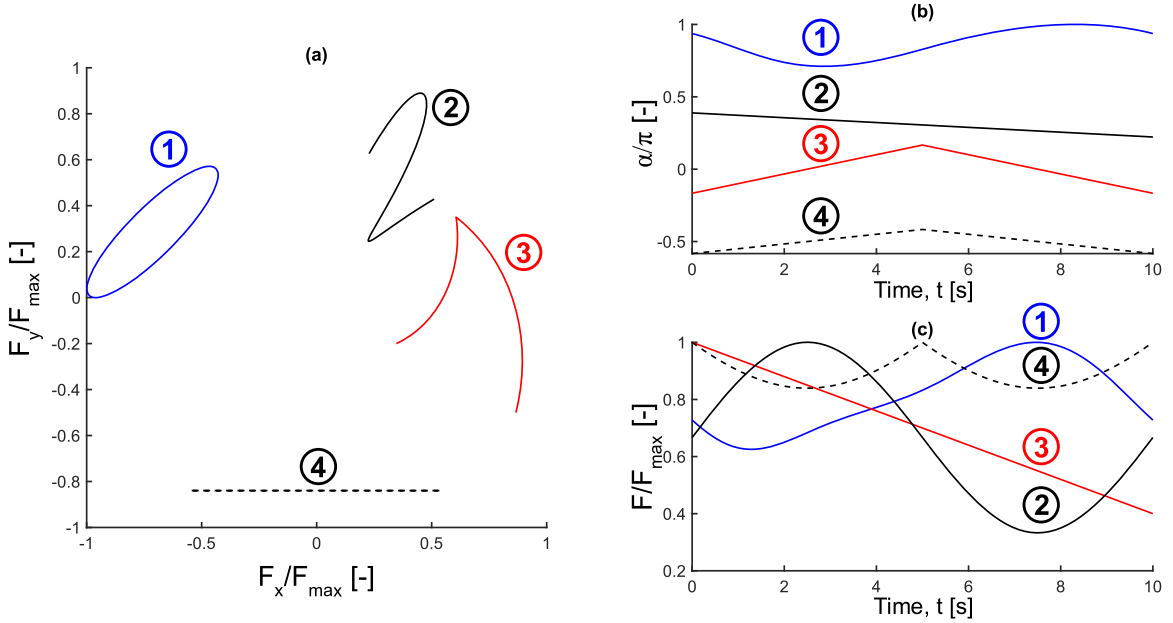

Fig. 12. Examples idealised cycles shown in (a) cartesian and (b-d) spherical coordinates: (1): Closed ellipse in cartesian plan; (2) Open Z in Cartesian plan: F-sinusoid with slow $\boldsymbol{\alpha}$ drift, (3) Open tooth in Cartesian plan: $\boldsymbol{\alpha}$-triangle wave with $\boldsymbol{F}$ drift, (4) Closed line/T-shape in Cartesian plan.

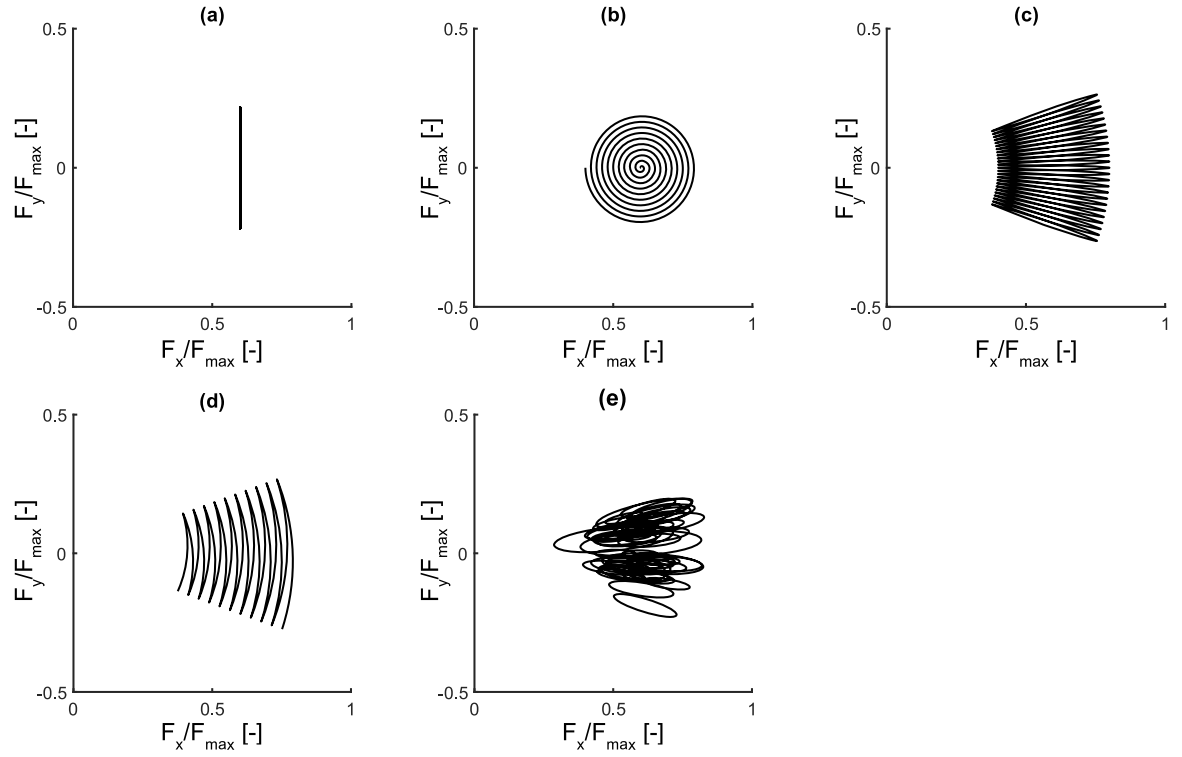

Fig. 13. Example idealised loading histories: (a) T-shape, (b) Offset spiral, (c) Fan, (d) Shell, (e) Random ellipses.

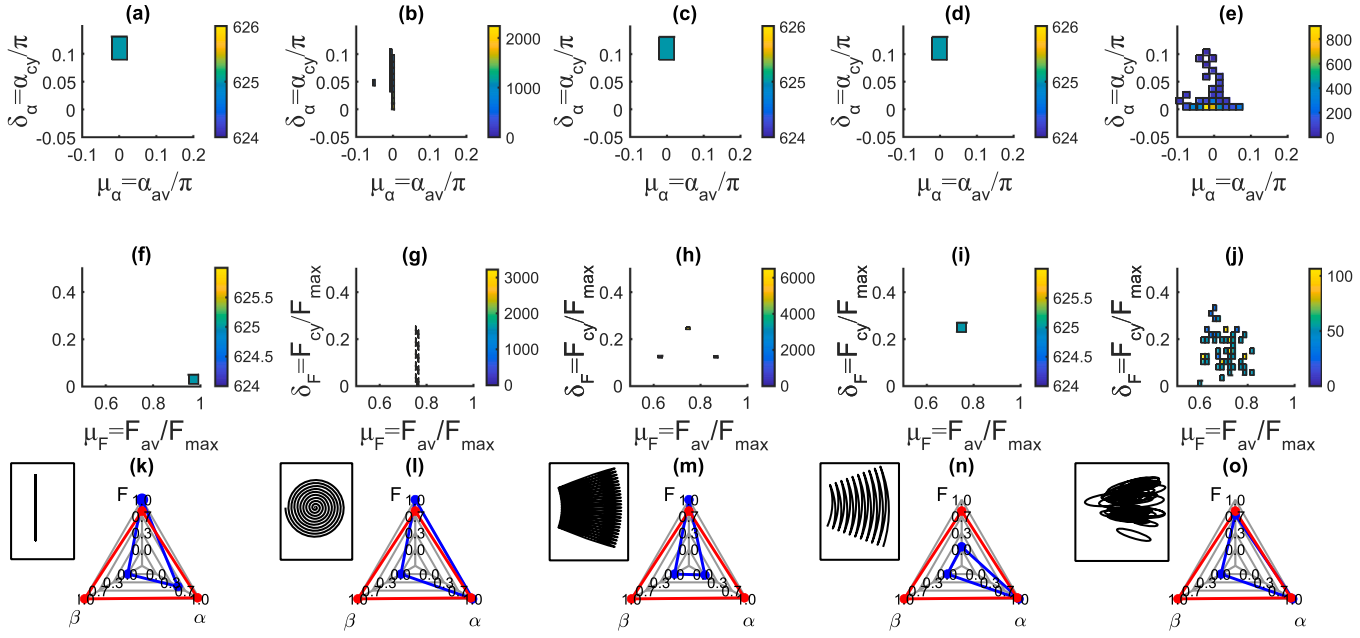

Fig. 14. 'Fingerprint' interpretation of idealised loading histories (a) T-shape, (b) Offset spiral, (c) Fan, (d) Shell, (e) Random ellipses.

useful for quantifying the similarity between actual and idealised load histories. The load history information is contained within the cyclic distribution functions, ψ, and the relative cyclic frequencies, ω. A simple measure of the similarity between two load histories can therefore be derived from the scalar sum of the difference in ψ of the two load histories, and the squared sum of the differences in relative cyclic frequencies. These similarity measures, between two load histories denoted I and II, are therefore given by:

$$\boldsymbol{S}_{\psi} = \begin{bmatrix} S_{\psi,F} \\ S_{\psi,\alpha} \\ S_{\psi,\beta} \end{bmatrix} = \begin{bmatrix} 1 - \frac{1}{2}\sum_{\delta_F}\sum_{\mu_F}\left|\psi_{F,I} - \psi_{F,II}\right| \\ 1 - \frac{1}{2}\sum_{\delta_\alpha}\sum_{\mu_\alpha}\left|\psi_{\alpha,I} - \psi_{\alpha,II}\right| \\ 1 - \frac{1}{2}\sum_{\delta_\beta}\sum_{\mu_\beta}\left|\psi_{\beta,I} - \psi_{\beta,II}\right| \end{bmatrix} \tag{1}$$

which can be simplified to a single scalar as

$$\widehat{S}_{\psi} = S_{\psi,F} \times S_{\psi,\alpha} \times S_{\psi,\beta} \tag{2}$$

and

$$S_{\omega} = \sqrt{\frac{1}{n}\sum_{i=1}^{n}\left(\omega_{I,i} - \omega_{II,i}\right)^2} \tag{3}$$

where the summation is over the n spherical components, ω_F, ω_α and ω_β.

The components of S_ψ and the scalar $\widehat{S}_\psi$ equal unity for exactly matching cyclic load histories and are zero if the cycles are entirely uncorrelated (i.e. they occupy separate zones of the cyclic heatmap, Fig. 7). Similarly, the scalar measure S_ω is zero if the cycles are wholly within different spherical parameters, and unity if the relative frequencies are identical.

These similarity measures are defined independent of any underlying geotechnical response. However, depending on the expected geotechnical response, there may be particular ranges or components of ψ and ω that have a greater influence than others on the strength, stiffness or accumulated displacement of the anchor. Where these influences are recognized, then a suitable weighting could be applied to the quantities used in the similarity measures.

To illustrate the comparison process, the similarity measures given by Eqs. (2) and 3 have been quantified for each idealised load path compared to the shared anchor time history (Fig. 15 and Table 2). High similarity is not expected for all the idealised paths, and the similarity measures show a wide range among the different cases. This demonstrates that the measures distinguish between the different 'fingerprints' of each loading history. In particular, the measures $\widehat{S}_\psi$ and S_ω are able to distinguish between aspects of the loading history beyond solely the temporal variation in load. For example, while the fan and shell cases have identical load heatmaps, their cyclic patterns are very different, due to the switching of the relative frequencies of F and α. This changes S_ω as well as altering the cyclic heatmaps, which influence $\widehat{S}_\psi$.

The idealized load paths that show best similarity with the shared anchor loading history are the offset spiral and the random ellipses, as shown by the similarity values being closer to zero in Fig. 15. These cases are distinct from the shell, fan and T-shaped cases in having a wider distribution of cyclic parameters and a closer match between the relative frequencies of each spherical parameter. These two features cause the function ψ and the vector ω of those two idealized patterns (shown on Fig. 14) to overlap with the same for the shared anchor (Fig. 7, Fig. 8a).

These results show that these simple scalar similarity measures provide a general quantitative basis for comparing two load histories, whether idealised or from floating system simulations. The framework therefore provides a valuable basis to support the development of

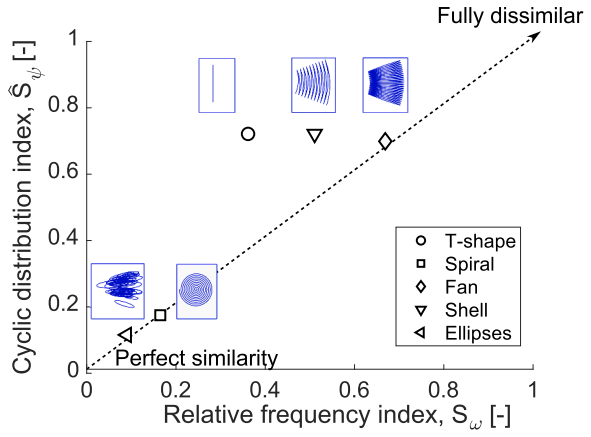

Fig. 15. Similarity scores of idealised loading histories compared to shared anchor example.

Table 2
Similarity measures between example case of shared anchor loading and idealised load paths (Fig. 12).

Name	Similarity measure	
	Relative frequency index, S_ω	Cyclic distribution index, $\widehat{S}_\psi$
T-shape	0.361	0.709
Offset spiral	0.165	0.163
Fan	0.669	0.687
Shell	0.619	0.709
Random ellipses	0.089	0.103

improved load paths for geotechnical testing that are representative of real conditions. It also provides a simple quantitative measure of how the soil response explored in idealised tests might be relevant to the soil response in other loading situations.

This 'fingerprint' concept is a new methodological approach so has not yet been applied to a wide range of loading time histories, which is a limitation.A next step is to apply this method to the full range of loading histories that are typically generated for the full set of design load cases and seastates for a wind farm project. This experience will help to validate this new approach as a method to filter, compare and cluster a large set of loading histories, and identify those that are critical to the geotechnical anchor design. Similarly, the fingerprint approach can be applied to a suite of laboratory-scale anchor tests, in which different loading histories are applied and differing severities of geotechnical response are observed (e.g. accumulated displacement, or degradation of capacity). By investigating the level of correlation between the fingerprint parameters and the geotechnical responses, the new methodology could be validated and developed further.

7. Conclusions

This paper provides a new interpretation of general multi-directional time-varying anchor loading that captures the key aspects needed to bridge to geotechnical design. These key aspects, which define a 'fingerprint' of the loading history, are:

1. A normalised distribution, ψ, ('heatmap') of cycles in a spherical coordinate system, of the form used in geotechnical S-N 'fatigue' analysis, identifying the distribution of the means and amplitudes of all cycles.
2. A vector of the relative number of cycles of each spherical parameter, ω, to distinguish between different forms of cyclic loading that encompass the same loading space but through different cyclic patterns.
3. Scalar quantities that define the maximum load, F_{max}, and the overall cyclic frequency, f_p of the primary component of ψ.

Secondary aspects that support visualisation of the loading are:

1. The temporal distribution of the anchor load, expressed in spherical parameters, to illustrate the loading space encompassed.
2. The frequency distribution of each spherical parameter, if geotechnical rate effects are relevant.

All these features normalise such that time histories of different length and different maximum amplitude can be compared in a consistent manner. This allows comparisons between scaled model tests, reduced scale field tests and simulations of (or data from) full-scale systems.

Measures of similarity have been defined, based on the difference between the normalised features of a pair of time histories. This provides a new quantitative measure to compare the idealised patterns of loading used in model testing, field testing or laboratory element tests with the more complex patterns that are found in real data of anchor loading or

from numerical simulations of floating systems.

This new framework allows the wide range of anchor loading histories relevant to a floating wind system – including 10–100 load cases typically considered in design – to be distilled into simple measures ('fingerprints'). This provides a new approach that could allow more rapid identification of critical cases and more efficient and accurate idealisation for geotechnical modelling and design.

To quantify the usefulness of this framework, and gain confidence in its applicability, future steps include (i) applying the method to compare and cluster the design loading cases and loading histories in a project design, to assess whether this gives an efficient basis to identify critical load cases, and (ii) applying the method to compare responses in a laboratory-scale parametric study of anchor behaviour involving a range of loading histories with varying fingerprints, to assess whether the critical geotechnical responses correlate with particular fingerprint features.

Data availability statement

The data underlying this article will be made publicly available on completion of the TAILWIND project and can be requested from the corresponding author in the interim.

CRediT authorship contribution statement

D.J. White: Writing – original draft, Supervision, Methodology, Formal analysis, Conceptualization. **B. Cerfontaine:** Writing – review & editing, Visualization, Project administration, Data curation, Conceptualization. **A. Rashidi Mehrabadi:** Writing – review & editing, Methodology, Conceptualization. **S. Gourvenec:** Writing – review & editing, Supervision, Methodology.

Declaration of competing interest

The authors declare the following financial interests/personal relationships which may be considered as potential competing interests:

Benjamin Cerfontaine reports financial support was provided by European Union. Susan Gourvenec reports financial support was provided by Royal Academy of Engineering. David White reports financial support was provided by Engineering and Physical Sciences Research Council. If there are other authors, they declare that they have no known competing financial interests or personal relationships that could have appeared to influence the work reported in this paper.

Acknowledgments

This research also forms part of TAILWIND, an EU Horizon Europe project with financial support provided by the European Commission (Grant Agreement 101136195). David White acknowledges support from the EPSRC Supergen Offshore Renewable Energy Hub (grant EP/Y016297/1). Susan Gourvenec is supported by the Royal Academy of Engineering, under the Chairs in Emerging Technologies scheme and this study forms part of the activities of the Royal Academy of Engineering Chair in Emerging Technologies Centre of Excellence for Intelligent & Resilient Ocean Engineering (IROE) at the University of Southampton.

References

Allen, C., Viscelli, A., Dagher, H., Goupee, A., Gaertner, E., Abbas, N., Hall, M., Barter, G., 2020. Definition of the UMaine VolturnUS-S reference platform developed for the IEA wind 15-megawatt offshore reference wind turbine (NREL/TP–5000-76773,1660012. MainId 9434.

Andersen, K.H., 2015. Cyclic soil parameters for offshore foundation design. the third ISSMGE McClelland lecture. Front. Offshore Geotech. III 1, 5–82.

Aubeny, C., 2017. Geomechanics of Marine Anchors. CRC Press.

Biscontin, G., Pestana, J.M., 2001. Influence of peripheral velocity on vane shear strength of an artificial clay. ASTM Geotechn. Test. J. 24 (4), 423–429.

Brown, A., Stephens, A., Rabb, B., Connell, R., Upton, J., 2019. Including the impact of climate change in offshore and onshore metocean design criteria to ensure asset robustness. In: Proceeding of the 38th International Conference on Ocean, Offshore and Arctic Engineering, 2019. OMAE, Glasgow, Scotland.

Cerfontaine, B., White, D.J., Kwa, K., Gourvenec, S., Knappet, J., Brown, M., 2023. Anchors for floating offshore wind: current technologies and future innovations. *Ocean Eng.*, Spec. Ed. *Ocean Eng.* 279 (2023), 114327. https://doi.org/10.1016/j.oceaneng.2023.114327.

Cerfontaine, B., Gourvenec, S.M., White, D.J., 2024. Specificities of floating offshore wind turbines for risk and safety evaluation of anchoring systems. State-of-the-art report. In: Proceeding of the XVIII European Conference on Soil Mechanics and Geotechnical Engineering. Lisbon, pp. 154–166.

Cheng, X., Ibraim, E., Liu, H., Pisanò, F., Diambra, A., 2023. Large diameter laterally loaded piles in sand: numerical evaluation of soil stress paths and relevance of laboratory soil element testing. Comput. Geotech. 154, 105139.

Coughlan, K., Davis, M., Westgate, Z., Lee, J., Arwade, S., Martin, B., DeGroot, D., 2025. Design and analysis of shared anchor layouts for floating wind farms in deep waters. Ocean Eng. 320, 120208.

Coughlan, K., 2025. Github repository: 3-line and 6-line shared anchor systems in deep water. OpenFAST Model. https://github.com/kcoughlan/3v6line_shared_anchors_fow.

DNV, 2017a. DNV-RP-E301 Design and Installation of Fluke Anchors. Det Norske Veritas.

DNV, 2017b. DNV-RP-E302 Design and Installation of Plate Anchors in Clay. Det Norske Veritas.

DNV, 2017c. DNV-RP-E303 Design and Installation of Suction Anchors in Clay. Det Norske Veritas.

DNV, 2021. Floating Wind Turbine Structures. Standard DNVGL-ST-0119 Det Norske Veritas.

Festa, O., Gourvenec, S., Sobey, A., 2025. Comparative analysis of load reduction device stiffness curves for floating offshore wind moorings. Ocean Eng. 298, 117266. https://doi.org/10.1016/j.oceaneng.2024.117266.

Finnie, I.M.S., Randolph, M.F., 1994. Punch-through and liquefaction induced failure of shallow foundations on calcareous sediments. In: Proceeding of the, International Conference on Behaviour of Offshore Structures. BOSS'94, Boston, pp. 217–230.

Foglia, A., Zhou, Z., Wang, Y., Polanía, O., van den Berg, D., Olsen, C.L., Cerfontaine, B., White, D., Gourvenec, S., Cabrera, M., Gavin, K., Kolios, A., Laham, N., 2025. First steps towards sustainable-by-design anchors for floating offshore wind. In: Proceeding of the International Symposium on Frontiers in Offshore Geotechnics (ISFOG). https://doi.org/10.53243/ISFOG2025-239.

Fontana, C.M., Arwade, S.R., DeGroot, D.J., Myers, A.T., Landon, M., Aubeny, C., 2016. Efficient multiline anchor systems for floating offshore wind turbines. In: Proceeding of the International Conference on Ocean, Offshore and Arctic Engineering. Paper OMAE2016-54476.

Fontana, C.M., Hallowell, S.T., Arwade, S.R., DeGroot, D.J., Landon, M.E., Aubeny, C.P., Diaz, B., Myers, A.T., Ozmutlu, S., 2018. Multiline anchor force dynamics in floating offshore wind turbines. Wind Energy 21 (11), 1177–1190. https://doi.org/10.1002/we.2222.

Goldschmidt, M., Muskulus, M., 2015. Coupled mooring systems for floating wind farms. Energy Procedia 80, 255–262. https://doi.org/10.1016/j.egypro.2015.11.429.

Gourvenec, S., 2020. Whole-life geotechnical design: what is it? What's it for? So what? And what next?: keynote. In: Proceedings of the 4th International Symposium on Frontiers in Offshore Geotechnics. Deep Foundations Institute, pp. 206–246 ed.

Gourvenec, S., 2022. Whole life design: theory and applications of this new approach to offshore geotechnics. Journal of Indian Geotechnical Society. Springer Nature. https://doi.org/10.1007/s40098-022-00627-x. Special Issue.

Gourvenec, S., 2024. Offshore geotechnical challenges of the energy transition, special issue: accelerating the energy transition with energy geotechnics. J. Geomech. Energy Environ. https://doi.org/10.1016/j.gete.2024.100584.

Greaves, D., White, D.J., Noble, D.R., Jeffrey, H., Gilbert, J., Zhao, X., Byrne, B., Willden, R., Stallard, T., Mullings, H., Scott, B., Brennan, F., Thies, P., Richards, L., Henderson, K., Mascall, R., 2024. Offshore Renewable Energy Outlook, 2040. Report by the Supergen Offshore Renewable Energy Hub.

Hann, M., Greaves, D., Raby, A., 2015. Snatch loading of a single taut moored floating wave energy converter due to focussed wave groups. Ocean Eng. 96, 258–271.

Huang, T., O'loughlin, C., Gaudin, C., Tian, Y., Lu, T., 2020. Drained response of rigid piles in sand under an inclined tensile load. Geotechn. Lett. 10 (1), 30–37.

IEC, 2019. Wind energy generation systems— design requirements for floating offshore wind turbines. Wind Energy Generation Systems—Part 3-2. International Electrotechnical Commission.

IRENA, 2024. Floating Offshore Wind Outlook. International Renewable Energy Agency, Abu Dhabi.

ISO, 2025. Standard 19901-4: Oil and Gas Industries Including Lower Carbon Energy — Specific requirements for Offshore Structures Part 4: Geotechnical design Considerations. International Standardisation Organisation.

Jonkman, J., Sprague, M., 2026. OpenFAST | NWTC Information Portal. nd. https://nwtc.nrel.gov/openfast.

Kwa, K., Weymouth, G., White, D.J., Martin, C.M., 2021. Analysis of the added mass term in soil bearing capacity problems. Geotechn. Lett. 11 (1), 80–87.

Kwa, K.A., White, D.J., Tosdevin, T., Jin, S., Greaves, D., 2023. Whole-life modelling of anchor capacity for floating systems: the RSN–CSI approach. Appl. Ocean Res. 138, 103671. https://doi.org/10.1016/j.apor.2023.103671.

Lai, Y., Wang, L., Hong, Y., He, B., 2020. Centrifuge modelling of the cyclic lateral behavior of large-diameter monopiles in soft clay: effects of episodic cycling and reconsolidation. Ocean Eng. 200, 107048.

Leblanc, C., Houlsby, G., Byrne, B., 2010. Response of stiff piles in sand to long-term cyclic lateral loading. Geotechnique 60 (2), 79–90.

Levy, N.H., Einav, I., Hull, T., 2009. Cyclic shakedown of piles subjected to two-dimensional lateral loading. Int. J. Numer. Anal. Meth. Geomech. 33, 1339–1361. https://doi.org/10.1002/nag.775.

Liao, D., Zhu, S.-P., Correia, J.A.F.O., De Jesus, A.M.P., Veljkovic, M., Berto, F., 2022. Fatigue reliability of wind turbines: historical perspectives, recent developments and future prospects. Renew. Energy 200, 724–742, 2022ISSN 0960-1481.

Lind, S.J., Stansby, P.K., Rogers, B.D., 2016. Fixed and moored bodies in steep and breaking waves using SPH with the Froude–Krylov approximation. J. Ocean Eng. Mar. Energy 2 (3), 331–354.

Lovera, A., Coquio, T., Peyrard, C., 2025. Analysis of loads applied on floating wind turbines shared anchors. Ocean Eng. 324, 120627, 2025ISSN 0029-8018.

Ma, H., Deng, Y., Chang, X., 2024. Effect of long-term lateral cyclic loading on the dynamic response and fatigue life of monopile-supported offshore wind turbines. Mar. Struct., 103521

Mandolini, A., Diambra, A., Ibraim, E., 2021. Stiffness of granular soils under long-term multiaxial cyclic loading. Géotechnique 71 (9), 795–811.

McAdam, R.A., Buckley, R.M., Schranz, F., Byrne, B.W., Jardine, R.J., Kontoe, S., Liu, T., Vinck, K., Crispin, J.J., 2024. Monotonic and cyclic lateral loading of piles in low- to medium-density chalk. Géotechnique. Published ahead of print. https://doi.org/10.1680/jgeot.23.00484, 22 October 2024.

Miura, K., Miura, S., Toki, S., 1986. Deformation behavior of anisotropic dense sand under principal stress axes rotation. Soils Foundat. 26 (1), 36–52.

Mosquera-Mosquera, I.A., Simão, M.L., Videiro, P.A., Sagrilo, L.V.S., 2020. Evaluating the impact of climate change on offshore structures design: a practical case study. Appl. Ocean Res. 94, 101992.

Pillai, A.C., Gordelier, T.J., Thies, P.R., Dormenval, C., Wray, B., Parkinson, R., Johanning, L., 2022. Anchor loads for shallow water mooring of a 15 MW floating wind turbine — Part I: chain catenary moorings for single and shared anchor scenarios. Ocean Eng. 266. https://doi.org/10.1016/j.oceaneng.2022.111816, 2022Article 111816.

Randolph, M.F., Gourvenec, S.M., 2011. Offshore Geotechnical Engineering. Spon Press.

Rashidi-Mehrabadi, A., Cerfontaine, B., Gourvenec, S., White, D.J., 2025. Numerical investigation of multidirectional response of shared anchor piles for offshore wind. In: Proceeding of the International Conference on Frontiers in Offshore Geotechnics. Nantes.

Richards, I.A., Byrne, B.W., Houlsby, G.T., 2020. Monopile rotation under complex cyclic lateral loading in sand. Géotechnique 70 (10), 916–930.

Richards, I.A., 2019. Monopile Foundations Under Complex Cyclic Lateral Loading. University of Oxford. PhD Thesis.

Rudolph, C., Grabe, J., 2013. Untersuchungen zu zyklisch horizontal belasteten Pfählen bei veränderlicher Lastrichtung. Geotechnik 36 (2), 90–95.

Schafhirt, S., Page, A., Eiksund, G.R., Muskulus, M., 2016. Influence of soil parameters on the fatigue lifetime of offshore wind turbines with monopile support structure. Energy Procedia 94, 347–356.

Sheahan, T.C., Ladd, C.C., Germaine, J.T., 1996. Rate-dependent undrained shear behavior of saturated clay. J. Geotech. Eng., ASCE 122 (2), 99–108.

Shimada, K., Shiroeda, T., Hotta, H., van Phuc, P., Kida, T., 2018. An empirical design formula of a shared pile anchor for a floating offshore wind turbine. In: Grand Renewable Energy 2018 Proceedings, 2018. https://doi.org/10.24752/gre.1.0_159.

Xiao, J., Juang, C.H., Wei, K., Xu, S., 2014. Effects of principal stress rotation on the cumulative deformation of normally consolidated soft clay under subway traffic loading. J. Geotech. Geoenviron. Eng. 140 (4), 04013046.

Zhang, C., White, D.J., Randolph, M.F., 2011. Centrifuge modelling of the cyclic lateral response of a rigid pile in soft clay. ASCE J. Geotech. Geoenviron. Engineering 137 (7), 717–729.

Zhou, Z., O'Loughlin, C.D., White, D.J., Stanier, S.A., 2020. Improvements in plate anchor capacity due to cyclic and maintained loads combined with consolidation. Geotechnique 70 (5), 448–467.